Dispersion of Micro Fibrillated Cellulose (MFC) in Poly(lactic acid) (PLA) from Lab-Scale to Semi-Industrial Processing Using Biobased Plasticizers as Dispersing Aids

Giovanna Molinari [1], Vito Gigante [1,2], Stefano Fiori [3], Laura Aliotta [1,2,*] and Andrea Lazzeri [1,2,*]

[1] Department of Civil and Industrial Engineering, University of Pisa, 56122 Pisa, Italy; giovanna.molinari@phd.unipi.it (G.M.); vito.gigante@dici.unipi.it (V.G.)

[2] Consorzio Interuniversitario Nazionale per la Scienza e Tecnologia dei Materiali (INSTM), 50121 Florence, Italy

[3] Condensia Quimica, C/Junqueras 11-A, 08003 Barcelona, Spain; s.fiori@condensia.com

[*] Correspondence: laura.aliotta@dici.unipi.it (L.A.); andrea.lazzeri@unipi.it (A.L.)

Abstract: In the present study, two commercial typologies of microfibrillated cellulose (MFC) (Exilva and Celish) with 2% wt % were firstly melt-compounded at the laboratory scale into polylactic acid (PLA) by a microcompounder. To reach an MFC proper dispersion and avoid the well-known aglomeration problems, the use of two kinds of biobased plasticisers (poly(ethylene glycol) (PEG) and lactic acid oligomer (OLA)) were investigated. The plasticizers had the dual effect of dispersing the MFC, and at the same time, they counterbalanced the excessive stiffness caused by the addition of MFC to the PLA matrix. Several preliminaries dilution tests, with different aqueous cellulose suspension/plasticizer weight ratios were carried out. These tests were accompanied by SEM observations and IR and mechanical tests on compression-molded films in order to select the best plasticizer content. The best formulation was then scaled up in a semi-industrial twin-screw extruder, feeding the solution by a peristaltic pump, to optimize the industrial-scale production of commercial MFC-based composites with a solvent-free method. From this study, it can be seen that the use of plasticisers as dispersing aids is a biobased and green solution that can be easily used in conventional extrusion techniques.

Keywords: polymer composites; biodegradable polymers; processing technologies

1. Introduction

In the 21st century, the need of finding new substitute materials, to minimize environmental footprint, is ever more pressing due to many ecological issues [1,2]. Nowadays, there is growing interest in biobased materials, especially for food packaging applications, to substitute the currently used petrochemical-based polymers. Among them, polylactic acid (PLA) has gained interest, because it can be synthesized from natural resources [3]. PLA can be used for single-use items that are used at room temperature, e.g., plastic utensils, cold-drink cups, thermoformed lunch boxes which are not reusable plasticware, plastic films, or, and rubber toughened for frozen applications [4,5]. Nevertheless, its poor flexibility, impact resistance, thermal stability during processing, and crystallization rates limit its applications [6]. A common sustainable technique to improve the final performances of PLA is related to different strategies, such as the development of natural-fiber-reinforced biocomposites [7–11]. Biocomposites show an improvement of both mechanical properties and thermal stability with respect to neat biopolymers.

In particular, cellulose is known to improve the barrier and mechanical properties of thermoplastic biopolymer films [12]. Actually, special interest has been paid to microfibrillated cellulose (MFC). MFC is a stereoregular linear polysaccharide of ringed glucose molecules with flat ribbon-like conformation. It is characterized by repeated D-glucopyranose units linked by 1,4-β glycoside bonds with particles sizes ranging from

50 to 180 μm [13]. Each microfibril is characterized by two different domains: one water-insoluble crystalline domain and a second amorphous region, having a weaker internal bonding. By considering an exploitable industrial MFC based biocomposites production, some critical issues have to be overcome. First of all, a proper cellulose dispersion and distribution is necessary for biocomposites that can exhibit the improvement of physical and mechanical properties [14].

However, the achievement of a cellulose suitable for dispersion is a critical issue due to its polar surfaces and its high specific surface area-to-volume ratio that makes it difficult to disperse in a nonpolar medium [15,16]. Since cellulose is essentially hydrophilic, it is clearly not easy to disperse it in a hydrophobic PLA matrix [17,18] due to the difficulty of organizing them in bundle, leading to some drawbacks such as aggregation and inefficient crystallization and strengthening. Once in the presence of these drawbacks, the final biocomposites are vulnerable to environmental attacks such as water absorption, biodeterioration, and mechanical failure at the interface [19].

To overcome agglomeration problems, in the literature, good results have been obtained on a laboratory scale, with some trials in a semi-industrial scale [20–23] or even in 3D printing [24], using environmentally unfriendly solvents or chemicals (acetone, methanol, acetic acid, chloroform, sulphuric acid, dimethyl acetamide, and lithium chloride), making the industrial-scale production of MFC-based biocomposites difficult and unsustainable.

Industrial producers of cellulose, such as Borregaard and Daicel Corp. that commercialize Exilva and Celish MFC, respectively, provide MFC in aqueous suspension. Consequently, once dried, it is very difficult to re-hydrate MFC, due to the irreversible agglomeration of polymeric fibrils and chains [25]. On the other hand, the use of MFC in aqueous solutions can cause PLA hydrolytic degradation, due to the reduction of its molecular weight, occurring by the random cleavage of the –C–O– ester bond by water molecules. By using an extruder equipped with venting and/or stripping systems and low extruder residence time, PLA hydrolytic degradation can be avoided as also reported in the literature by Taheri et al. [26].

It is noteworthy that by removing water in the melt, MFC agglomeration can occur. For this reason, a good solution can be a plasticizer addition to the aqueous suspension, to be used as a dispersing agent for MFC [27]. Furthermore, the plasticiser could be able not only to enhance the PLA/cellulose interface, with the formation of H-bonding or dipolar interactions, but also to uniform the cellulose dispersion. Indeed, as evidenced by Khalil et al. [28], the mechanical properties of PLA are increased, when cellulose nanofibrils and a low-molecular weight plasticizer such as poly(ethylene glycol) (PEG) are added to the matrix. This phenomenon shows that the addition of PEG gives positive effects because it acts as a compatibilizer improving interaction fibrils distribution, avoiding also matrix hydrolysis due to the presence of a water-based solution of cellulose [29,30].

The choice for plasticizers (specially in packaging applications) is strongly limited by technical and legislative requirements (FSA A03070, FCN 1926), based on their compatibility, biodegradability, and toxicity. In the literature, several plasticizers have been added to PLA such as triacetin, citrate esters, glycerol, malonate oligomers, adipates and polyadipates, PEG, poly(propylene glycol) (PPG), or their copolymers [31,32]. Among different plasticizers available in the market, oligomeric acid lactic (OLA) has been considered as an effective plasticizer for PLA, due to their comparable chemical structure and its renewable nature. A good miscibility between PLA and OLA can be obtained thanks to their close solubility parameters, being 17.7 $MPa^{1/2}$ for OLA and in the range of 19.5 $MPa^{1/2}$ to 20.5 $MPa^{1/2}$ for PLA [33,34]. PEG was also investigated because, as reported by Kloser et al. [35], it is able to graft onto the MFC surface (forming covalent bonds), inhibiting their aggregation. Moreover, PEG was used as a steric stabilizer in the preparation of dispersible fillers also by Cheng et al. [36]. Furthermore, the water polarity value, higher than those of PEG and OLA, implies that polymer–plasticizer/oligomer–filler interactions are more favored than those of polymer–water–plasticizer/oligomer–filler ones, with a subsequent decrease of the polymer hydrolytic degradation.

The aim of this work is to study an efficient method to industrialize the production of MFC-based biocomposites with good dispersion within a PLA matrix. For this purpose, a systematic study was carried out to find the optimum plasticizer/MFC ratio. A first laboratory-scale investigation was carried out, and the best plasticizer ratio was scaled-up into a semi-industrial twin-screw extruder to validate the processing.

2. Materials and Methods

2.1. Materials

The materials used in this work were as following:

- Extrusion-grade poly(lactic) acid 2003D purchased from NatureWorks (D-content: between 3% and 6%; density: 1.24 g/cm^3; molecular weight of 200,000 g/mol and melt flow index of 6 g/10 min at 190 °C and 2.16 kg);
- PEG 400 purchased from Sigma-Aldrich (CAS number: 25322-68-3; MW: 400 g/mol; density: 1.12 g/cm^3; water solubility: 100 mg/mL).
- LAO (trade name: Glyplast OLA 2) provided by Condensia Quimica, (Barcelona, Spain): it is a completely biodegradable and impact modifier PLA plasticiser (ester content: >99%; density: 1.10 g/cm^3; viscosity (ASTM D 445): 90 mPa·s at T = 40 °C, water content (ASTM E 203): maximum 0.1%; molecular weight: 500 g/mol [37]);
- MFC Exilva F 01-L 10% provided by Borregaard (Sarpsborg, Norway) had a solid content of 1.5–2.4% and a viscosity in H$_2$O (2%, mPa·s) of ≥14,000.
- MFC Celish KY100S 25% purchased from Daicel Miraizu Ltd. (Osaka, Japan) (CAS number: 9004-34-6; density: 1.27–1.61 g/cm^3).

2.2. Neat MFCs Characterizations

Preliminary characterizations on the two types of MFCs were carried out.

From a thermal point of view, a thermogravimetric analysis (TGA) was carried out in order to ensure that no degradation occurred during extrusion compounding. The TGA of MFC was performed on a TA Q-500 (TA Instruments, Waters LLC, New Castle, DE, USA). About 15 mg of the sample were put into a platinum pan and heated at a scanning velocity of 10 °C/min from room temperature up to 1000 °C, using nitrogen as purge gas. Before their characterization, both MFCs were dried by the solvent evaporation technique according to the procedure also adopted in [38,39]. The suspensions were put inside a vacuum oven and dried at 130 °C for 5 h.

On the MFCs (dehydrated with the same procedure described above for the TGA), ATR (Attenuated total reflection) spectra were recorded at room temperature in the 400–4000 cm^{-1} range, by means of a Nicolet 380 FT-IR spectrometer (Thermo Fisher Scientific, Madison, WI, USA) equipped with a smart iTX ATR accessory.

The morphologies of both neat MFCs were investigated by a FEI ESEM Quanta 450 FEG instrument (Thermo Fisher Scientific, Waltham, MA, USA). The samples, after being dried with the same procedure adopted for TGA measurements, were sputtered with a thin layer of platinum by using a sputter coater Leica EM ACE600, to make them conductive and to avoid charge buildup prior to the observation.

2.3. Microcompounding of Lab-Scale PLA/MFCs Composites

At the beginning, both the MFC solutions were diluted with water, until the achievement of a suspension containing an equal content (2 wt %) of MFC. Both the microcellulosic suspensions were stirred for 5 min, until a qualitative observation of dispersion/homogenization was reached. After the dilution, different amounts of plasticizers were added to the MFC/waters suspensions. The emulsions were mechanically mixed by the use of an IKA T 25 digital ULTRA-TURRAX® Disperser (Staufen, Germany). Each mixture was stirred at 8000 rpm for 210 s in order to disperse and homogenize the plasticizers with microcelluloses. The obtained mixtures were stored at 5 °C to inhibit the inherent dehydration, because, once dried, could lead to an irreversible agglomeration of both microcellulose fibrils and chains [24].

These emulsions were fed together with PLA granules in a Haake Minilab II (Thermo Scientific Haake GmbH, Karlsruhe, Germany) co-rotating conical twin-screw extruder to obtain different composites having a fixed MFC content but with different plasticizers amounts. The microcompounding was also carried out on PLA containing different amounts of plasticizers as a reference. The microcompounding was carried at T of 190 °C and 100 rpm (torque of 91 N/m at 34 bar) for a residence time of 210 s. The formulations are reported in Table 1.

Table 1. Formulations names and compositions.

Formulation	Poly(lactic acid) (PLA)	Poly(ethylene glycol) 400 (PEG 400; wt %)	Oligomeric Acid Lactic 2 (OLA 2; wt %	Exilva F-01 L wt %	CELISH KY100S wt %
PLA_PEG_5	95	5	/	/	/
PLA_PEG_10	90	10	/	/	/
PLA_PEG_15	85	15	/	/	/
PLA_OLA_5	95	/	5	/	/
PLA_OLA_10	90	/	10	/	/
PLA_OLA_15	85	/	15	/	/
PLA_PEG_5_EX	93.1	4.9	/	2	/
PLA_PEG_10_EX	88.2	9.8	/	2	/
PLA_PEG_15_EX	83.3	14.7	/	2	/
PLA_OLA_5_EX	93.1	4.9	/	2	/
PLA_OLA_10_EX	88.2	9.8	/	2	/
PLA_OLA_15_EX	83.3	14.7	/	2	/
PLA_PEG_5_CE	93.1	/	4.9	/	2
PLA_PEG_10_CE	88.2	/	9.8	/	2
PLA_PEG_15_CE	83.3	/	14.7	/	2
PLA_OLA_5_CE	93.1	/	4.9	/	2
PLA_OLA_10_CE	88.2	/	9.8	/	2
PLA_OLA_15_CE	83.3	/	14.7	/	2

The strand coming out of the microextruder was then cooled, pelletized and dried in a ventilated oven at 60 °C for 24 h.

The pellets were molded through a NOSELAB ATS (Milano, Italy) compression-moulding machine, to obtain films with a thickness of 200 μm. The parameters adopted were as following: plates temperature of 190 °C, pressure of 5 metric tons, and residence time of 4 min. No change of colour was observed after the compression moulding manufacturing process, indicating that no degradation occurred [40]. The films were placed in a controlled atmosphere chamber at a temperature of 25 °C and a relative humidity of 50% for 48 h before further characterizations.

2.4. Scale-Up of PLA/MFCs Composites Extrusion Compounding

For the formulations that had excellent dispersion and the best compromise between mechanical properties and easy processability, the extrusion compounding was scale-upped on a semi-industrial Comac EBC 25HT (L/D = 44) (Comac, Cerro Maggiore, Italy), twin-screw extruder. A schematization of the extrusion compounding configuration is reported in Figure 1. In Figure 1, mass flows are also reported, which show how the total amount of water in the emulsion is stripped by the degassing system.
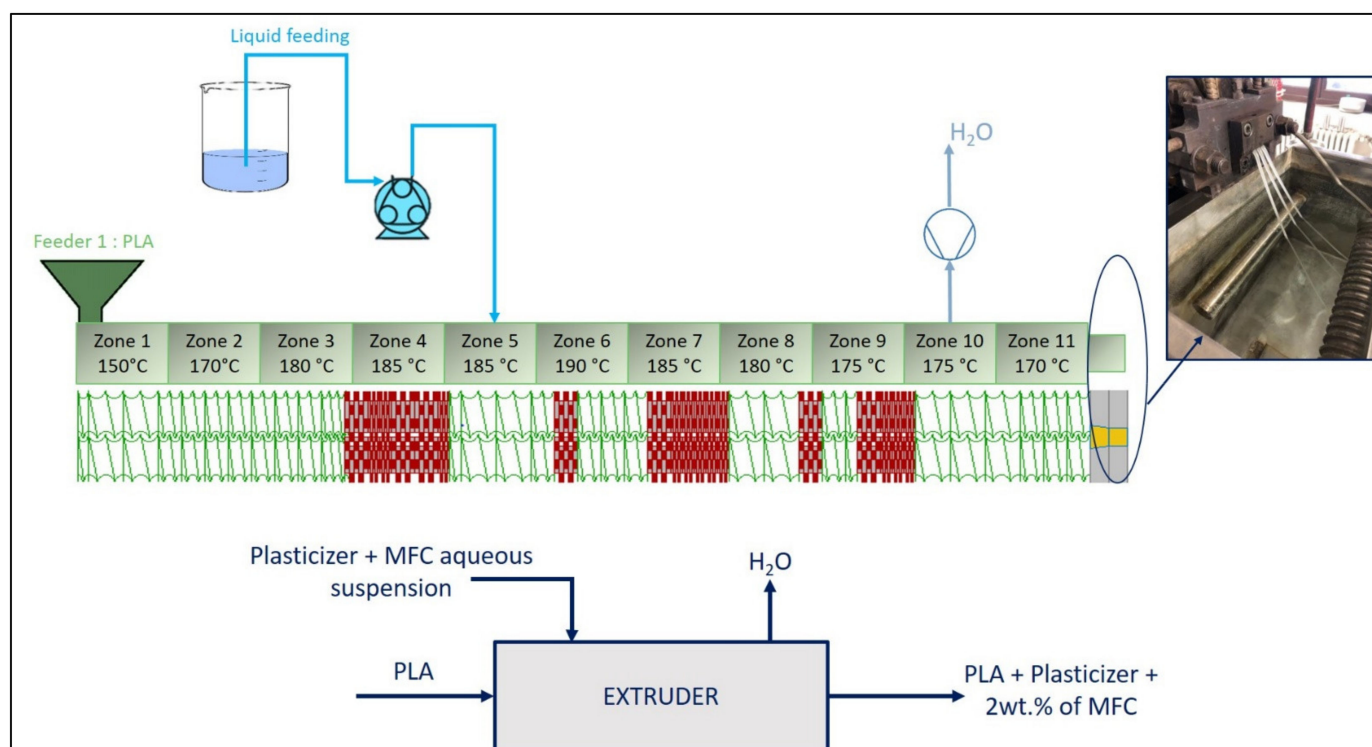
Figure 1. Schematization of the inlet and outlet flows in a semi-industrial twin-screw extruder coupled with the temperature profiles and the screws configuration.

After the die exits, the granule composition is given by PLA, the plasticizer, and MFC. The strands coming out of the extruder were cooled in a water bath and then pelletized by an automatic cutter. The granules were then dried in a DP604–615 PIOVAN dryer (Venezia, Italy) at 60 °C for 16 h, and compression-molded films were obtained following the same procedure described in Section 2.3.

2.5. Mechanical Characterization

From compression-molded films, ISO 527-2 type A dumbbell specimens were cut with a Manual ELASTOCON Cutting Press EP 08 (Brahmult, Sweden) to carry out tensile tests at room temperature with an INSTRON 5500R Universal Testing Machine (Canton, MA, USA) equipped with a 100 N load cell at 50 mm/min and interfaced with MERLIN software (INSTRON version 4.42 S/N–014733H). At least 10 specimens were tested for each formulation according to the ASTM D 638. The main mechanical properties (stress at break, elongation at break, and yield stress) were obtained, and the average values were reported.

The evaluation of the elastic moduli for all formulations was carried out on a Gabo Eplexor® (Ahlden, Germany) with a 100 N load cell. At least five specimens were tested for each sample. During the test, the constant temperature and frequency were 25 °C and 1 Hz, respectively.

2.6. Optical Characterization

The films morphology was investigated with a FEI ESEM Quanta 450 FEG instrument (Thermo Fisher Scientific, Waltham, MA, USA) after sputtering the film fracture surface with a thin layer of platinum, by using a sputter coater Leica EM ACE600 before the investigation.

2.7. FT-IR Characterization

ATR spectra were recorded on the compression-moulded films for each lab-scaled composite formulation, at room temperature in the 400–4000 cm^{-1} range, by means of a

Nicolet 380 FT-IR spectrometer (Thermo Fisher Scientific, Madison, WI, USA) equipped with a smart iTX ATR accessory.

2.8. Thermal Characterization

On the scale-upped formulations, differential scanning calorimetry (DSC) analysis was carried out on a DSC Q200 TA-Instrument (New Castle, UK) equipped with an RSC (radiative sky cooler) cooling system. For all measurements, nitrogen was adopted as purge gas (set at 50 mL/min). The instrument was calibrated with indium used as a standard for temperature and enthalpy calibration. The materials used for DSC were cut from the compression-moulded films. The samples, having masses between 10 and 15 mg, were sealed inside aluminium hermetic pans. In order to take into account the thermal history of the samples and to know the final crystallinity obtained, only one heating run was carried out. The samples were heated from room temperature to 200 °C at 10 °C/min and held at 200 °C for 1 min. The melting temperature (T_m) and the cold crystallization temperature (T_{cc}) of the blends were determined by considering the maximum of the melting peaks and the minimum of the cold crystallization peak, respectively. While the melting and cold crystallization, enthalpies were determined from the corresponding peak areas in the thermograms. The crystallinity percentage of PLA was calculated according the following equation:

$$X_{cc,PLA} = \frac{\Delta H_{m,PLA} - \Delta H_{cc,PLA}}{\Delta H^{\circ}_{m,PLA} \cdot W_{PLA}}, \tag{1}$$

where $\Delta H_{m,PLA}$ and $\Delta H_{cc,PLA}$ are the melting enthalpy and the enthalpy of cold crystallization of *PLA*, respectively, while *WPLA* is the *PLA* weight fraction in the formulation; $\Delta H^{\circ}_{m,PLA}$ is the melting enthalpy of the 100% crystalline *PLA* (equal to 93 J/g [41]).

2.9. Melt Flow Characterization

Melt flow rate (MFR) and melt volume rate (MVR) measurements were carried out according to UNI EN ISO 1133 by a CEAST Melt Flow Tester MF20 (Instron, Canton, MA, USA). Five grams of pellets obtained by upscale extrusion were heated at 190 °C in a barrel and extruded through a normalized die (2.095 mm) under a constant load of 2.16 kg.

## 3. Results and Discussion

3.1. Neat MFCs Results

The TGA thermograms of the dried celluloses (in Figure 2) showed that the cellulose decomposition started at 300 °C and persisted until 370 °C, where the maximum weight decrease occurred at 355 °C. The results obtained are in accordance with other studies related to MFC typologies [42,43]. At 400 °C, almost all celluloses were pyrolyzed. A small weight loss (3 wt %) was found in the range of 25–200 °C correlated to the evaporation of the humidity residual after the drying process, higher than that of the Exilva ones.

The degradation behavior of the Celish was similar to that of the Exilva, and for both samples, a pyrolyzed residue corresponding to 20 wt % of the initial weight was detected at 700 °C.

Regarding the ATR-FTIR results, the analysis in Figure 3 revealed the absorption bands at 2918 and 2891 cm^{-1} that are related to symmetric and asymmetric C–H vibrations of all hydrocarbon constituents in polysaccharides. Within the region 1630–1100 cm^{-1}, there are the typical bands assigned to cellulose. The absorption located at 1633 cm^{-1} is related to the C–O double bond corresponding to the vibration of water molecules absorbed in cellulose. The vibrations at 1460 and 1425 cm^{-1} are attributed to the –CH$_2$– group, within the crystalline structure of cellulose (the vibrations associated to the amorphous cellulose are generally located in the bending region of the IR spectra). The absorption at 1633 cm^{-1} is related to the C–O double bond. The vibration at 1163 cm^{-1} is assigned to the C–O–C antisymmetric bridge stretching vibration.
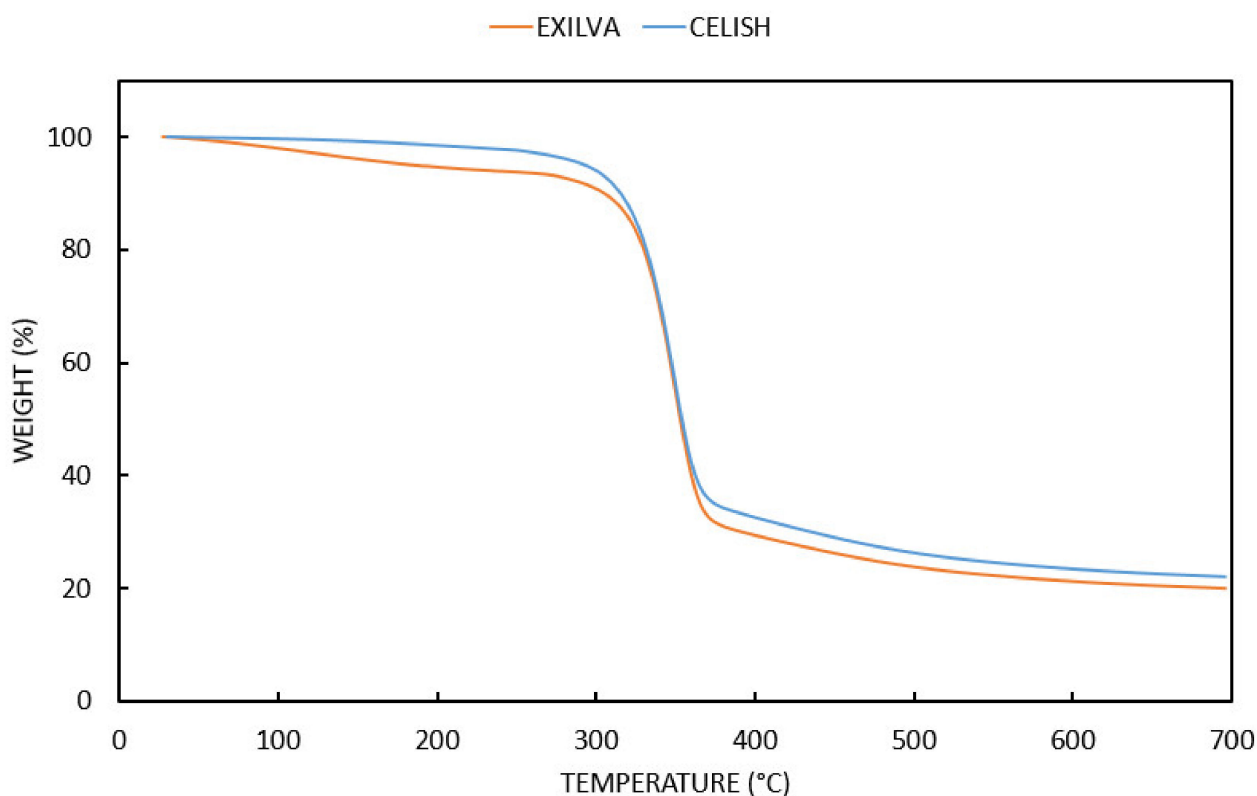
Figure 2. Thermogravimetric analysis (TGA) thermograms of Exilva F 01-L and Celish KY100S.
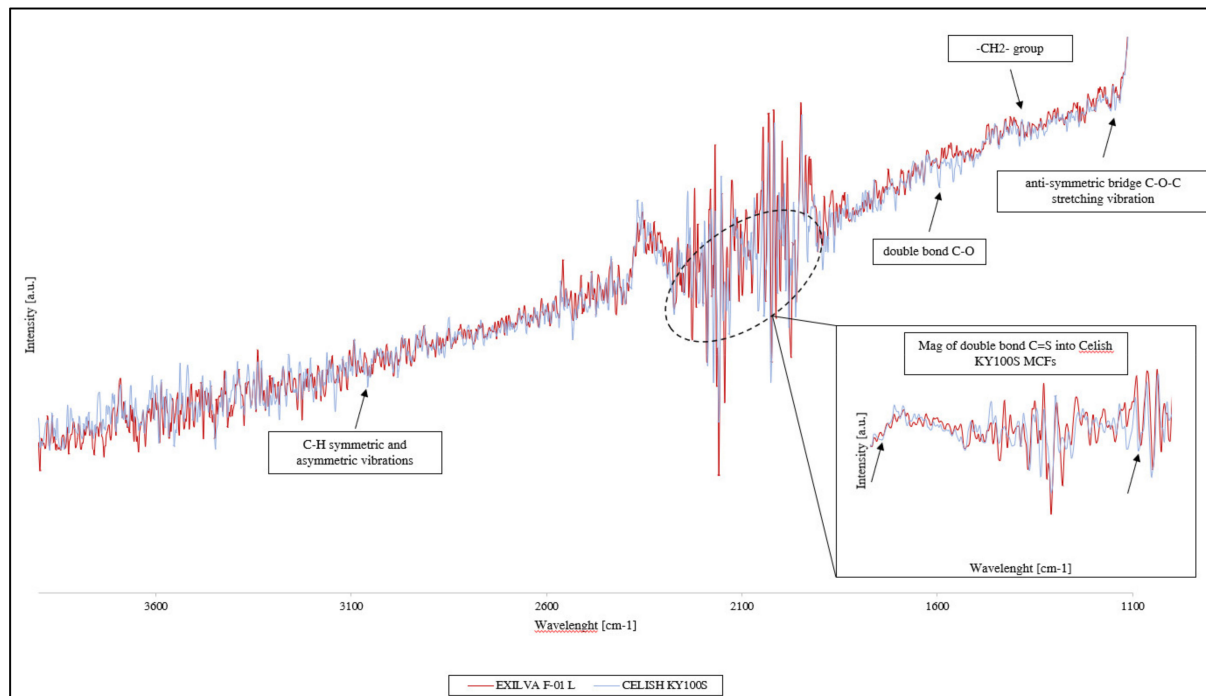

Figure 3. ATR-FTIR spectra of Exilva F 01-L, Borregaard, and Celish KY100S.

For the Celish–MFC samples, the only difference is related to the presence of the vibrations at 2333 and 2003 cm^{-1}, ascribable to the C=S double bond, derived from a possible preparation by sulfuric acid hydrolysis, absent in the Exilva–MFC samples.

The morphologies of the pure MFC–Celish and MFC–Exilva samples, obtained after the drying process described in Section 2.2, are reported in Figures 4 and 5 respectively.

Both MFC types consisted of long and thin fibers arranged in a three-dimensional network interconnected to each other. The fibers size was wide with some fibers having a nanoscale diameter and others being bigger with microscale diameters. Karim et al. have demonstrated that for this type of MFC, a wide distribution of diameter dimensions is present [44].
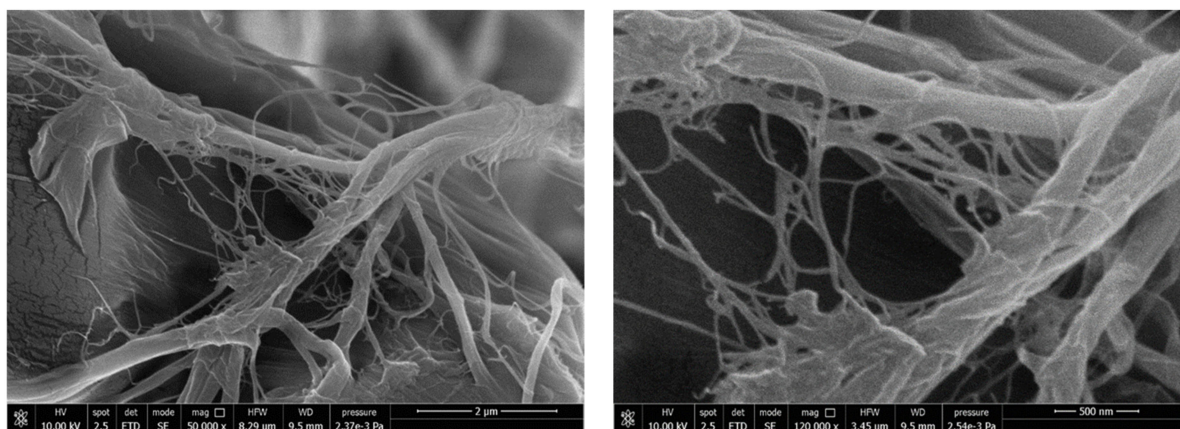
Figure 4. Morphology of the Celish–micro fibrillated cellulose (MFC) sample.
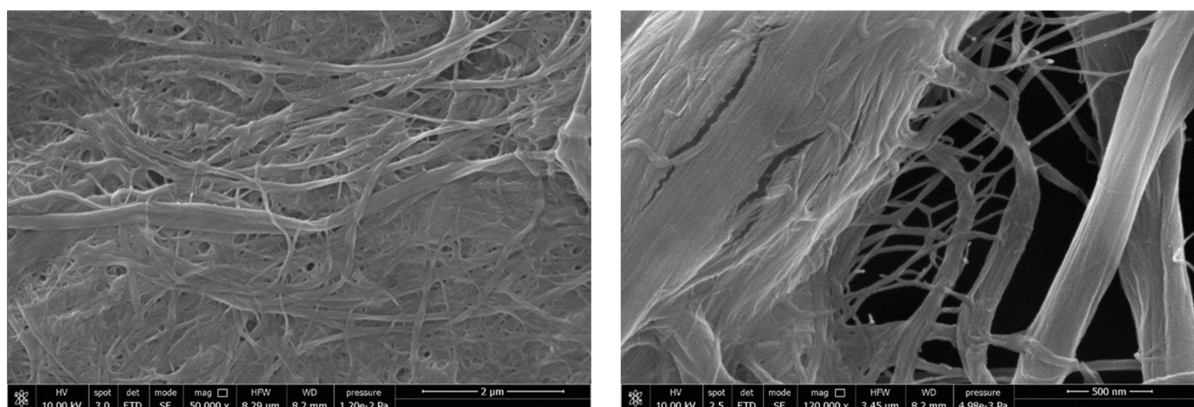
Figure 5. Morphology of the Exilva–MFC sample.

In the literature, it has been shown [45,46] that as much as 38% of the total Exilva MFC population is in the form of fibrils with diameter of less than 100 nm. The Celish–MFC sample alternatively appeared as bundles and single fibrils having widths between 30 nm and 100 nm in accordance with what can be found in the literature [47].

3.2. Lab-Scale Results

The results of the first mechanical tests are reported in Table 2. It was observed that an increasing plasticisers amount added to the PLA matrix led to a decrease of the elastic modulus compared to pure PLA, as reported in the literature for the same PLA grade [6]. The MFCs addition counterbalanced this effect by increasing the elastic modulus comparable or even higher than pure PLA. Furthermore, this material stiffness increment was proportional to the plasticizer content; this effect is probably correlated to the MFC dispersion improvement with the plasticizer amount. As also reported in the literature for plasticized filled systems, there is a balance between the stiffness increment caused by the MFC introduction and the plasticizing effect of OLA 2 or PEG 400 [48–51]. In the literature, it was observed that reinforcing fillers such as MFC are capable of improving PLA properties. However, the mechanical properties decreased with increasing MFC content due to its poor dispersion and subsequent chain restriction movement [52]. In contrast, in this case, the mechanical properties were increased, when plasticizers were added to

the PLA/MFC system. Besides, used as a plasticizer, PEG also acted as a compatibilizer between the PLA matrix and cellulose nanofibrils to improve their interaction and prevent aggregation [53].

Table 2. Tensile properties of lab-scale films production.

| Formulation	Elastic Modulus (GPa)	σ_{break} (MPa)	ε_{break} (%)
PLA_PEG_5	2.47 ± 0.48	23.87 ± 2.72	11.98 ± 0.31
PLA_OLA_5	2.51 ± 0.02	24.03 ± 2.74	19.8 ± 0.98
PLA_PEG_5_EX	3.31 ± 0.02	53.12 ± 3.33	3.92 ± 0.18
PLA_OLA_5_EX	3.06 ± 0.80	53.16 ± 1.10	2.92 ± 0.11
PLA_PEG_5_CE	2.76 ± 0.33	46.68 ± 4.46	3.76 ± 0.09
PLA_OLA_5_CE	3.07 ± 0.50	51.66 ± 2.04	3.15 ± 0.10
PLA_PEG_10	2.07 ± 0.31	23.05 ± 2.62	18.1 ± 0.52
PLA_OLA_10	2.15 ± 0.28	21.63 ± 1.11	42.78 ± 0.87
PLA_PEG_10_EX	3.39 ± 0.03	46.49 ± 2.14	4.61 ± 0.27
PLA_OLA_10_EX	3.17 ± 0.13	49.63 ± 1.44	3.36 ± 0.04
PLA_PEG_10_CE	2.97 ± 0.44	46.80 ± 3.15	3.88 ± 0.02
PLA_OLA_10_CE	3.68 ± 0.17	51.59 ± 2.77	3.23 ± 0.04
PLA_PEG_15	1.63 ± 0.78	18.48 ± 0.2	30.45 ± 5.26
PLA_OLA_15	1.64 ± 0.4	20.02 ± 0.54	49.95 ± 1.22
PLA_PEG_15_EX	3.53 ± 0.07	43.18 ± 2.44	5.52 ± 0.28
PLA_OLA_15_EX	3.45 ± 0.43	44.76 ± 1.13	3.56 ± 0.14
PLA_PEG_15_CE	3.54 ± 0.30	47.06 ± 3.79	3.88 ± 0.04
PLA_OLA_15_CE	3.81 ± 0.23	42.98 ± 2.04	3.62 ± 0.08

The use of plasticizers enhanced the ductility of the matrix favoring plastic deformation, as evidenced by the increment of elongation at break with the plasticizer amount. The MFC addition modified the mechanical behavior of the films from ductile to brittle due to the stiffening of the material by increasing the stress at break. On the other hand, the drawback is the lowering of the elongation at break of the material. Taking into account the deviations obtained, the stress at break of the plasticized MFC composites was quite constant and did not seem to vary with the plasticizer amount.

On the basis of the mechanical properties obtained, by underlining the importance of the plasticizer in improving the MFC dispersion and considering its stiffness balancing, the formulations with the highest plasticizer content (14.7 wt %) were selected for the scale-up.

The MFC dispersion into the plasticized PLA matrix can be evaluated from the SEM images reported in Figure 6, Figure 7, Figure 8, even if the SEM resolution was deemed insufficient to add morphological insight as stated also by Kvien et al. [54]. With the addition of MFCs, a rougher surface was observed. This morphology is consistent with the presence of plasticizers [55]. A little plastic deformation and a few long threads of a deformed material were noticeable. Some of very thin and long polymer fibrils spanned over the surface, which was probably the origin of a plastic fracture mechanism that allows the material to yield and form long PLA "fibrils", can be observed. The "fibrils" seemed broken and buckled, falling onto the fractured surface [56]. However, these "fibrils" should not be confused with the cellulose fibrils which, by contrast, reinforced the polymer matrix. Additionally, the micrographs showed some different characteristic diameter tangles of cellulose fibrils, probably related to their mutual macromolecular self-organising during the biosynthesis process, of which the modification and destruction would cause defibrillation, forming looser structures [57]. Interesting is the random and well-dispersed presence of shiny dots within the plasticized matrix [58], corresponding to the transverse fractured sections of cellulose fibril and, as evidenced previously, its enhanced defibrillation [59]. From the SEM micrographs, it is possible to conclude that the plasticisers adopted allow a good MFCs dispersion within the polymeric matrix without leading to the formation of significant agglomerates that could result in detrimental mechanical properties.
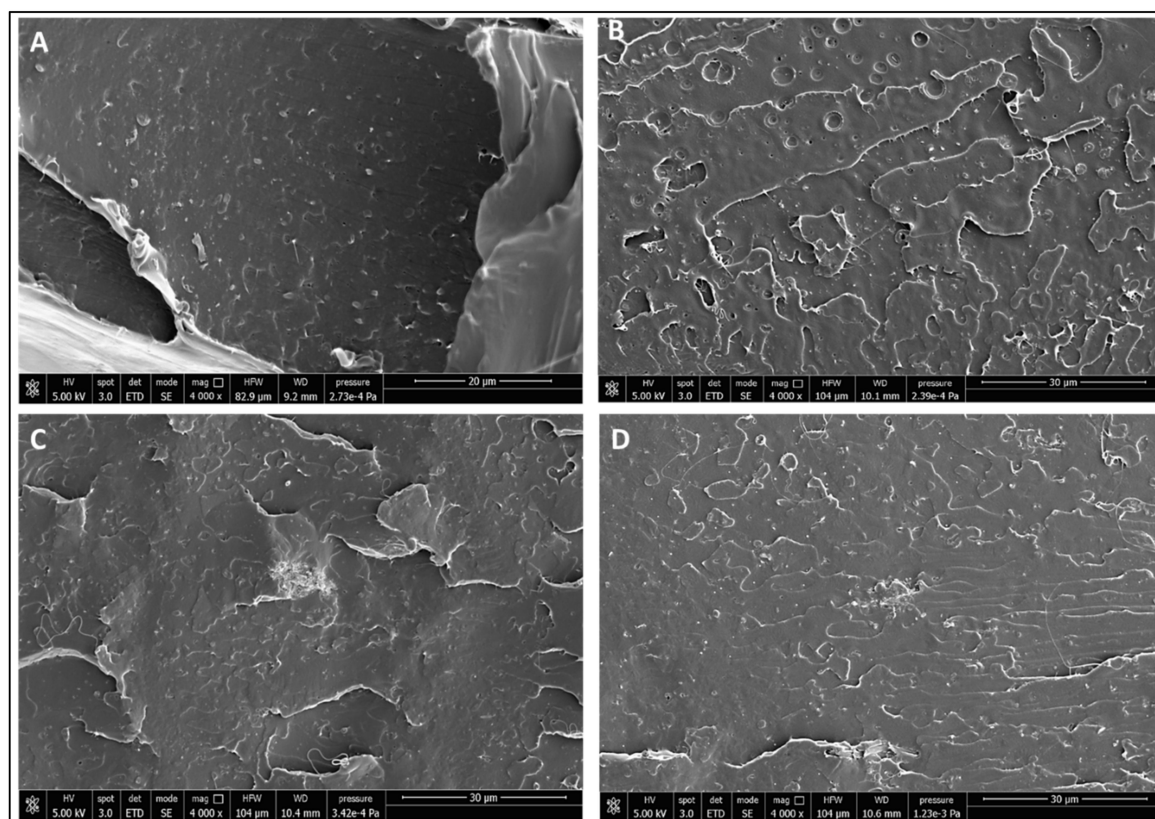
Figure 6. SEM micrographs of PLA_PEG_5_EX (**A**), PLA_OLA_5_CE (**B**), PLA_PEG_5_EX (**C**), and PLA_OLA_5_CE (**D**) at a magnification of 4000×.
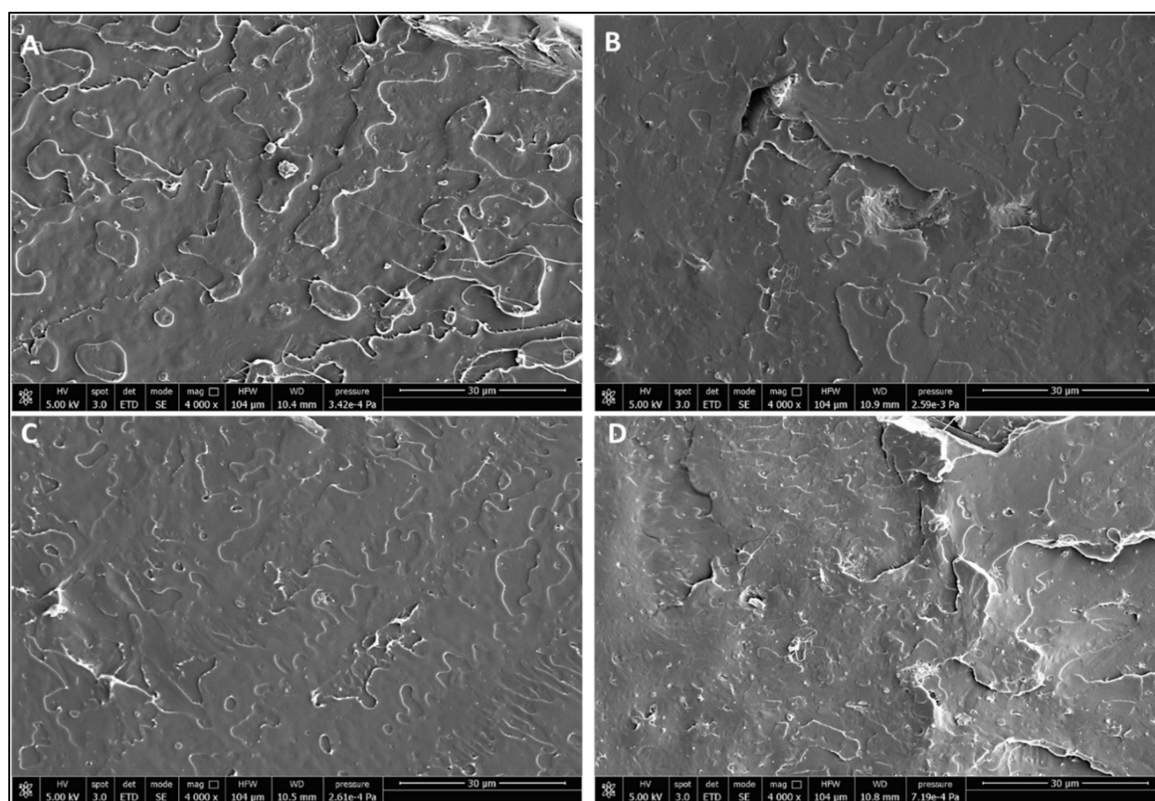
Figure 7. SEM micrographs of PLA_PEG_10_EX (**A**), PLA_OLA_10_CE (**B**), PLA_PEG_10_EX (**C**), and PLA_OLA_10_CE (**D**) at a magnification of 4000×.
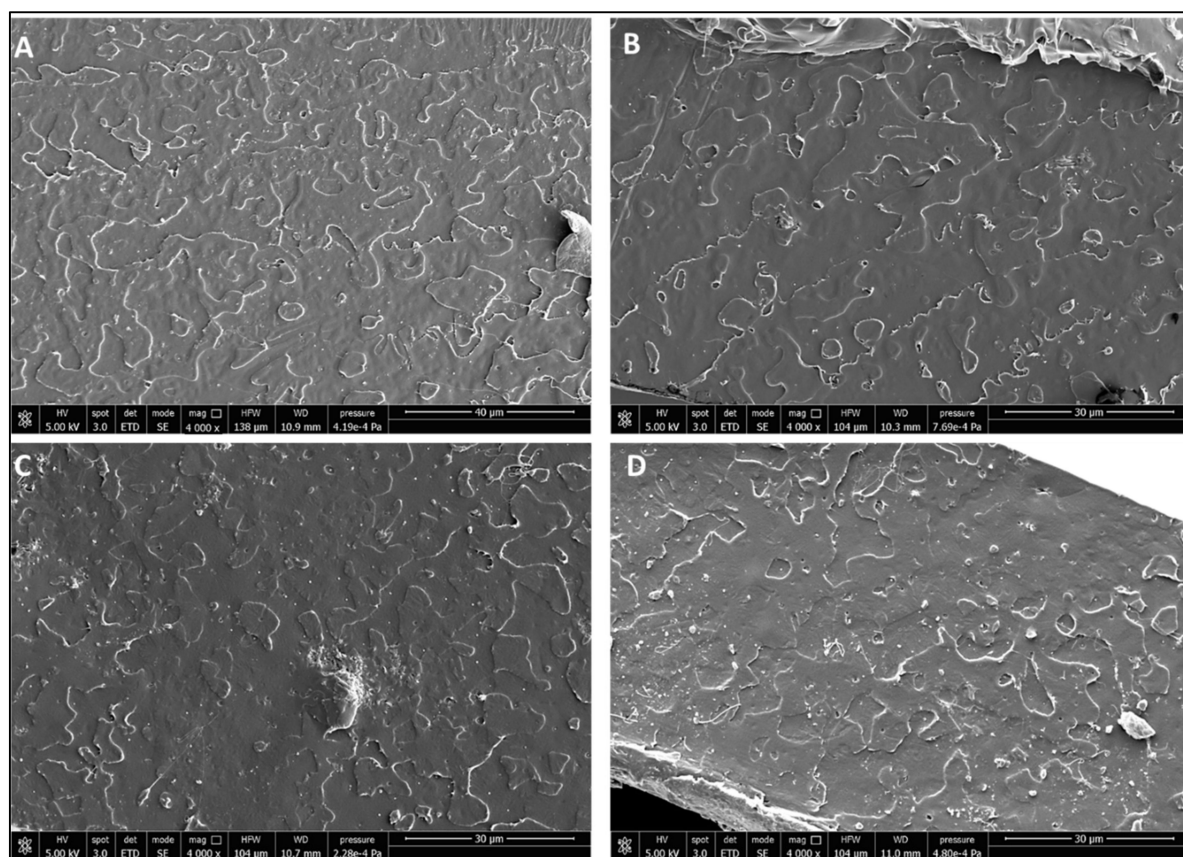
Figure 8. SEM micrographs of PLA_PEG_15_EX (**A**), PLA_OLA_15_CE (**B**), PLA_PEG_15_EX (**C**), and PLA_OLA_15_CE (**D**) at a magnification of 4000×.

The ATR-FTIR spectra in Figure 9 showed the regions allowed identifying the interactions within the composites. The first region appeared with the IR peaks at 1780 and 1680 cm^{-1}, ascribed to the characteristic carbonyl (–C=O) stretching peak of PLA. The second region is related with –C–O– bond stretching in the –CH–O– group of PLA at about 1180 cm^{-1}, which is associated with the C–O–C stretching. Finally, the last region is associated with the peaks at about 1180, 1128, 1082, and 1041 cm^{-1} of C–O–C stretching vibrations. Generally, these characteristics peaks are also found in the literature [60,61]. The spectra containing PEG 400 and OLA 2 appeared to be similar, showing the presence of almost the same functional groups. Most of the ATR-FTIR bands associated with the PLA and PEG 400 or OLA 2 at least partially overlapped with other bands in the spectra. For example, the CH stretching bands at 2800–3000 cm^{-1} of the methyl groups in the PLA and the methylene groups of the PEG partially overlapped, as well as with the C–O–C bands of the PLA and OLA 2, which appeared in the range from 1050 to 1250 cm^{-1}. Nevertheless, the peak at 1750 cm^{-1} related to the carbonyl stretching of the product esters was absent in the composites with PEG 400. The results can be justified with the higher sensitivity of ester groups to hydrolysis.
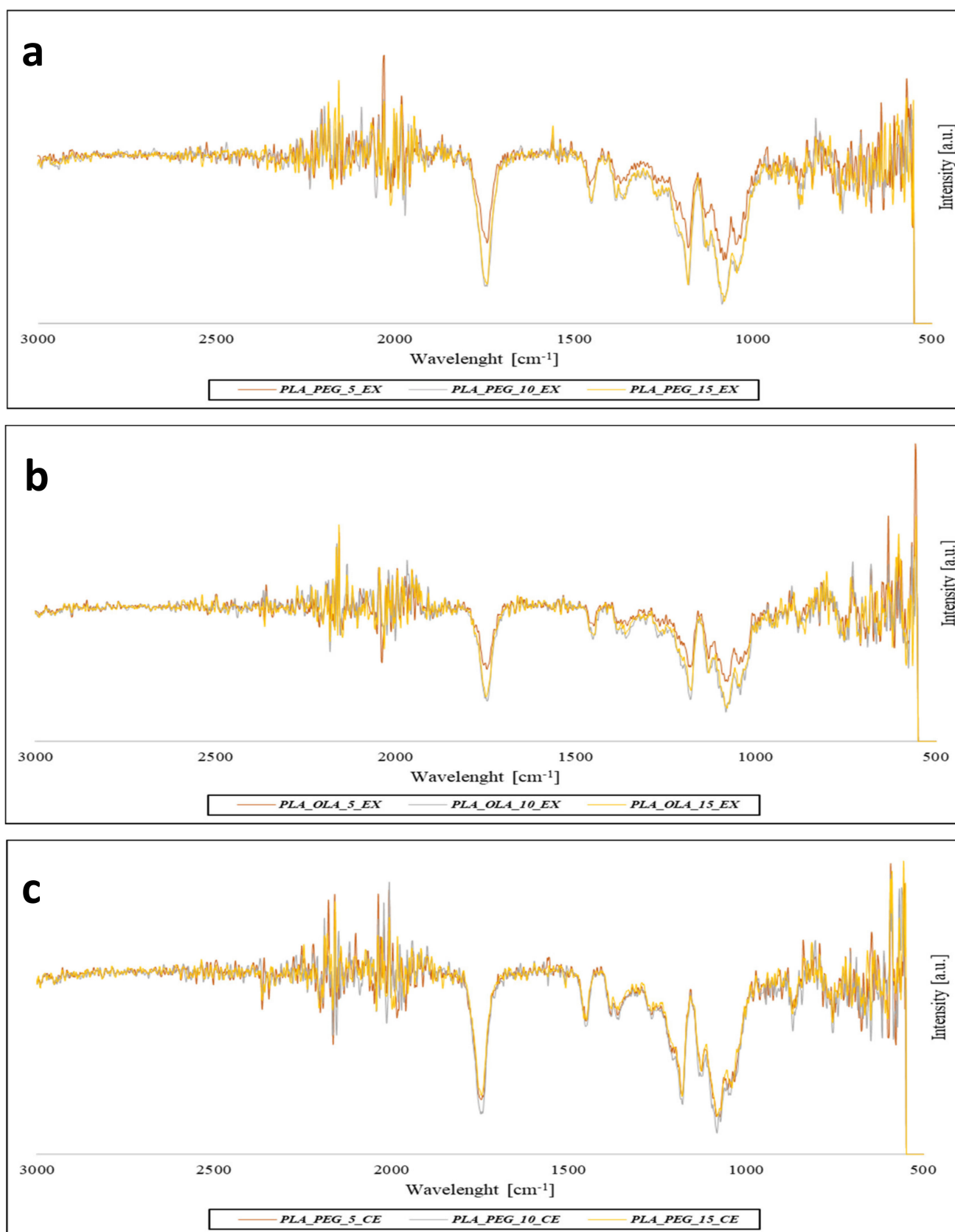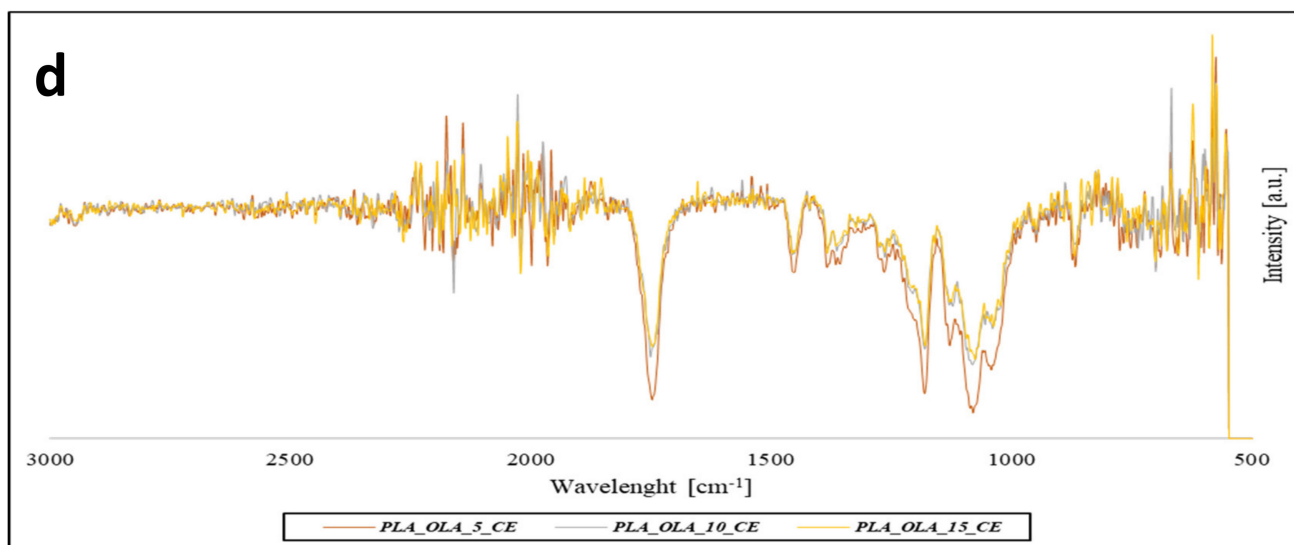
Figure 9. *Cont.*

Figure 9. ATR-FTIR spectra of PLA_PEG-EX (**a**), PLA_OLA_EX (**b**), PLA_PEG_CE (**c**), and PLA_OLA_CE (**d**) formulations with different amounts of plasticizers.

The plasticized PLA/MFC composites spectra displayed all the characteristic bands of the plasticized biopolymer, except for the absence of the peak at 1680 cm^{-1}, related to the carbonyl stretching of the product esters. This revealed that there is not only a physical interaction [62] between the PLA and MFCs, but also a new chemical bonding interaction between the plasticized matrices and the cellulose. The two plasticizers probably improved the interaction between the polar surface of the cellulose and the apolar biopolymer. The –COOH, C–O–C, and O–H plasticizers groups allowed the formation of H-bonding or dipolar interactions between the matrix and the MFCs (as depicted in Figure 10). The new type of bond proposed would explain the absence of the classic C=O absorption peak into the IR spectra of all the composites.
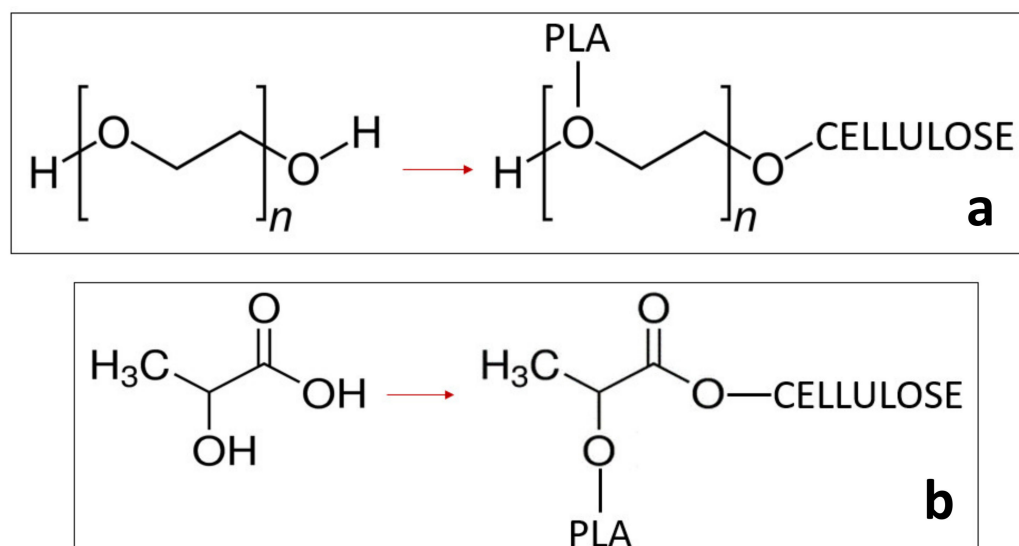
Figure 10. (**a**) Proposed PEG 400 composite chemical structure; (**b**) proposed OLA 2 composite chemical structure.

3.3. Scale-Up Results

The results of the granules obtained in the lab scale are very promising, because without the use of harmful solvents it is possible to obtain biocomposite formulations with a good dispersion of cellulose within a polymer matrix. Consequently, it was decided to carry out the scale-up on blends with a 15% plasticizer, which have good mechanical properties but also look good enough to be fed into a semi-industrial extruder by means of a peristaltic pump. Figure 11 shows a brief outline of the steps from the creation of the emulsion to feeding into an extruder.
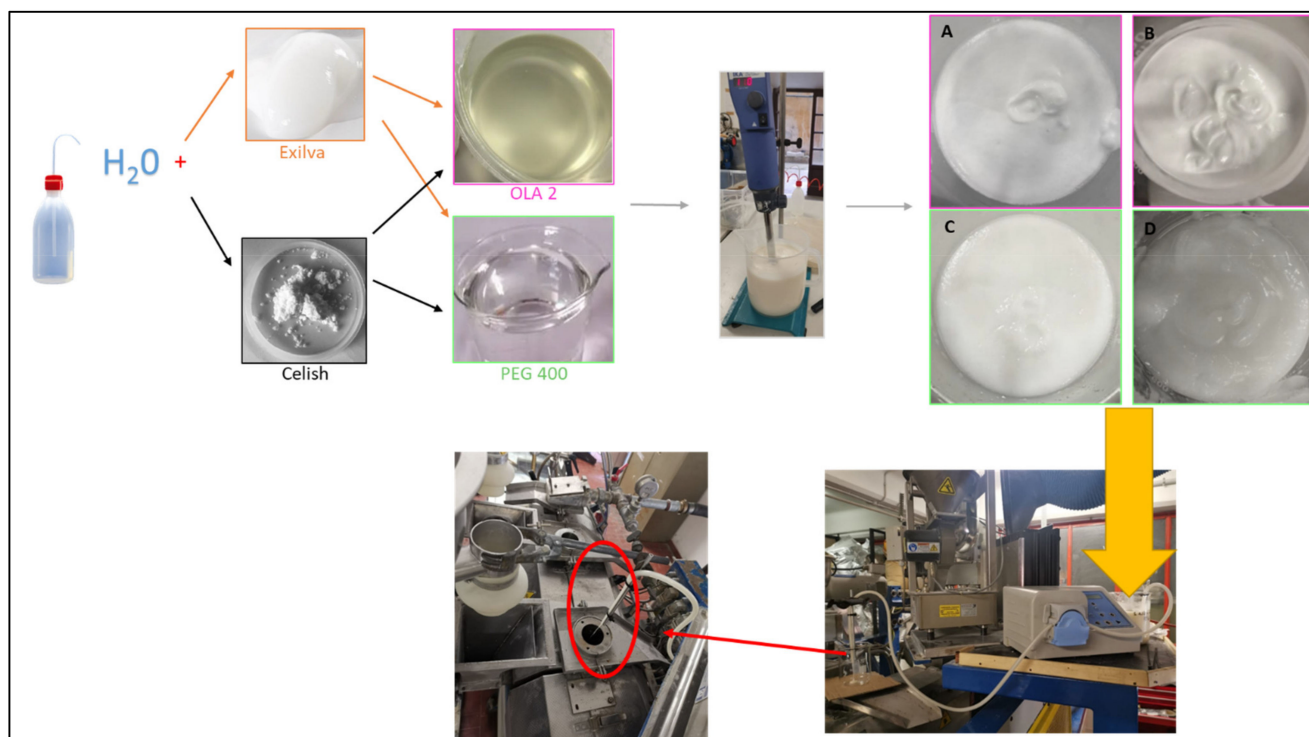
Figure 11. Scheme of the emulsion preparation with MFCs, OLA, and PEG to achieve OLA_15_EX (**A**), OLA_15_CE (**B**), PEG_15_EX (**C**), and PEG_15_CE (**D**). The emulsion emission in the semi-industrial extruder through a peristaltic pump is also shown.

The mechanical properties of the up-scaled formulation are described in Table 3. The formulations were named in the same way but with an asterisk added to differentiate them from lab-scaled formulations.

Table 3. Tensile properties of the up-scaled film formulations.

Formulation	Elastic Modulus (GPa)	σ_{break} (MPa)	ε_{break} (%)
PLA_OLA_15*	0.73 ± 0.01	8.03 ± 0.89	178.3 ± 18.2
PLA_PEG_15*	1.15 ± 0.05	10.85 ± 1.51	149.6 ± 21.3
PLA_PEG_15_EX*	2.16 ± 0.19	19.84 ± 1.04	23.91 ± 3.06
PLA_OLA_15_EX*	2.50 ± 0.16	28.44 ± 2.22	11.84 ± 4.52
PLA_PEG_15_CE*	2.11 ± 0.14	19.32 ± 2.37	11.79 ± 0.13
PLA_OLA_15_CE*	2.13 ± 0.07	29.03 ± 1.39	15.16 ± 2.65

The mechanical properties of the films produced with the semi-industrial extruded granules showed a similar trend of those of the lab-scaled films. The MFC addition, also in this case, increased the elastic modulus and the stress at break and decreased the elongation at break. Despite the trend similarity, it can be observed that for both the plasticized PLA matrix and the plasticized matrix with MFCs, the plasticizing effect was more marked.

Comparing the mechanical data, it can be observed that the up-scaled formulations had a lower elastic modulus and tensile at break; on the other hand, they achieved a higher elongation at break. The presence of longer screws characterized by mixing elements that guarantee a better plasticization and a degassing system (that favors a more efficient water removal) led to the realization of a product with better characteristics compared to lab-scale ones.

The final formulations were also characterized from a thermal point of view: the thermograms are reported in Figure 12, while the main thermal properties are reported in Table 4.
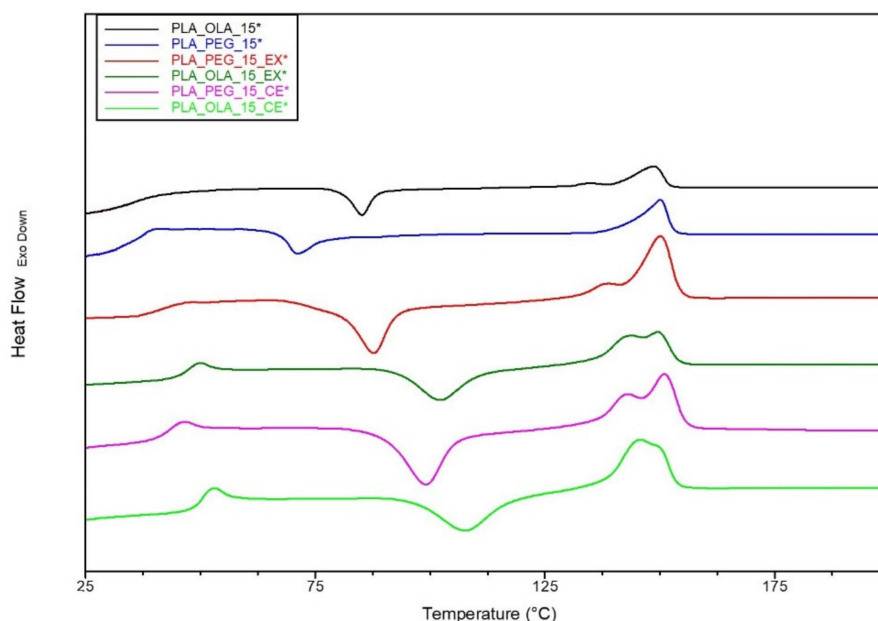
Figure 12. Differential scanning calorimetry (DSC) thermograms of the first-heating up-scaled film formulations.

Table 4. DSC results of the first-heating up-scaled film formulations.

Figure	T_g (°C)	T_{cc} (°C)	T_m (°C)	ΔH°_{cc} (J/g)	ΔH°_m (J/g)	X_{cc} (%)
PLA_OLA_15*	35.6	85.2	148.8	6.1	7.2	1.4
PLA_PEG_15*	37.2	70.9	150	5.8	10.8	6.3
PLA_PEG_15_EX*	40.5	87.6	150	20.9	28.3	9.5
PLA_OLA_15_EX*	45	102.2	149.4	14.9	22.2	9.4
PLA_PEG_15_CE*	43.3	99	150.9	25.7	32.9	9.2
PLA_OLA_15_CE*	50.4	107.9	148.3	18.7	25.7	9

As it can be expected, the plasticizer addition decreased the PLA glass transition temperature (that is around to 60 °C [63]). PEG and OLA 2 enhanced the PLA chain mobility, bringing PLA T_g values equal to 35.6 °C for OLA 2 and 37.2 °C for PEG 400; these values are consistent with what can be found in the literature [64,65]. Interesting is to observe how the addition of MFC increased the PLA glass transition temperature. This behavior can be ascribed to the MFC presence that, especially if they were well dispersed into the polymeric matrix, limited the polymeric chain motions. As far as the melting temperatures is concerned, no significant variations were found between the various formulations. On the other hand, the cold crystallization temperature showed differences that can be ascribable not only to the different types of plasticizer adopted, but also to the MFC addition. All formulations containing PEG 400 had a lower cold crystallization temperature if compared to their corresponding formulations with OLA 2. Probably the lower molecular weight [51] of PEG 400 compared to that of OLA 2 led to a better PLA chain

motion for PEG 400 instead of OLA 2. The MFC addition increased the cold crystallization temperature, making it more difficult for PLA to crystallize during the processing (as also confirmed from the crystallinity values obtained). This effect was also found in the literature, and it can be correlated to the partially amorphous cellulose that changes the crystallinity of PLA, increasing the disorder of the molecular chain [21]. MFCs interacted with the amorphous PLA phase and hindered the crystallization from the glassy state [66]. The crystallinity results showed a slight improvement of the PLA crystallinity that for all formulations containing MFC was around 9%.

A useful test to evaluate the processability of the studied formulations is the mass flow rate analysis. Firstly, from Figure 13, it can be seen that the matrices fluidity of the granules obtained in the extruder was much higher than those of all composites, showing that both the MFCs gave strength to the melt, as also reported for other fillers [67,68]. More specifically, the matrix plasticized with OLA had a tremendous fluidity at 190 °C with a rather low melt strength and was hardly used for filming applications at such temperatures. The melt strength was considerably improved with the inclusion of MFCs. The melt flow rate of the Exilva–MFC composite was even 5 times lower than that of the Celish–MFC composite. Exilva and Celish reinforced also the polymeric melt of the matrices plasticized with PEG.
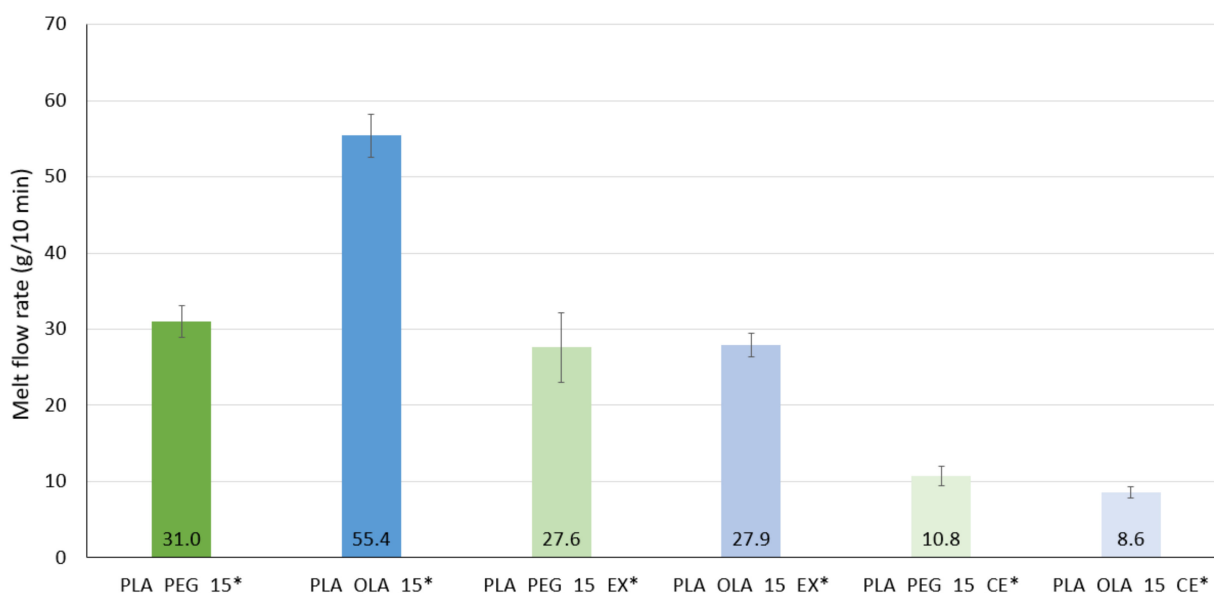

Figure 13. Mass flow rates (in g/10 min) of the up-scaled formulations achieved at 190 °C and with a weight of 2.16 kg.

4. Conclusions

In this study, the possibility to process successfully, at the semi-industrial scale, PLA-based composites containing MFC was investigated. In order to overcome the well-known MFC agglomeration drawback and at the same time to have a green manufacturing process (free-solvent approach), it was decided to investigate the use of two different typologies of biobased and biodegradable plasticizers (OLA 2 and PEG 400) as dispersing agents. Two different typologies of commercial MFC were investigated (Exilva and Celish) that were added with 2 wt % into a PLA matrix.

The study was first carried out at the laboratory scale by a microcompounder; from the first trial, the best plasticizer content that guaranteed the best compromise between mechanical properties and the MFC dispersion was chosen. The best formulation was then scaled up in a semi-industrial twin-screw extruder. The results obtained were very interesting. Thanks to the use of plasticizers, a good MFC dispersion and, at the same time, the stiffness loss imparted form the presence of the plasticizer was counterbalanced

by the MFC presence with no detrimental effect on the final mechanical properties of the biocomposites.

References

1. Botta, L.; Mistretta, M.C.; Palermo, S.; Fragalà, M.; Pappalardo, F. Characterization and Processability of Blends of Polylactide Acid with a New Biodegradable Medium-Chain-Length Polyhydroxyalkanoate. *J. Polym. Environ.* **2015**, *23*, 478–486. [CrossRef]
2. Bontempi, E.; Sorrentino, G.P.; Zanoletti, A.; Alessandri, I.; Depero, L.E.; Caneschi, A. Sustainable Materials and their Contribution to the Sustainable Development Goals (SDGs): A Critical Review Based on an Italian Example. *Molecules* **2021**, *26*, 1407. [CrossRef] [PubMed]
3. Gálvez, J.; Correa Aguirre, J.P.; Hidalgo Salazar, M.A.; Vera Mondragón, B.; Wagner, E.; Caicedo, C. Effect of Extrusion Screw Speed and Plasticizer Proportions on the Rheological, Thermal, Mechanical, Morphological and Superficial Properties of PLA. *Polymers* **2020**, *12*, 2111. [CrossRef]
4. Aversa, C.; Barletta, M.; Puopolo, M.; Vesco, S. Cast extrusion of low gas permeability bioplastic sheets in PLA/PBS and PLA/PHB binary blends. *Polym. Technol. Mater.* **2020**, *59*, 231–240. [CrossRef]
5. Pietrosanto, A.; Scarfato, P.; Di Maio, L.; Nobile, M.R.; Incarnato, L. Evaluation of the Suitability of Poly(Lactide)/Poly(Butylene-Adipate-co-Terephthalate) Blown Films fro Chilled and Frozen Food Packaging Applications. *Polymers* **2020**, *12*, 804. [CrossRef] [PubMed]
6. Gigante, V.; Canesi, I.; Cinelli, P.; Coltelli, M.B.; Lazzeri, A. Rubber Toughening of Polylactic Acid (PLA) with Poly(butylene adipate-co-terephthalate) (PBAT): Mechanical Properties, Fracture Mechanics and Analysis of Ductile-to-Brittle Behavior while Varying Temperature and Test Speed. *Eur. Polym. J.* **2019**, *115*, 125–137. [CrossRef]
7. La Mantia, F.P.; Morreale, M. Green composites: A brief review. *Compos. Part A Appl. Sci. Manuf.* **2011**, *42*, 579–588. [CrossRef]
8. Aliotta, L.; Gigante, V.; Coltelli, M.B.; Cinelli, P.; Lazzeri, A. Evaluation of Mechanical and Interfacial Properties of Bio-Composites Based on Poly (Lactic Acid) with Natural Cellulose Fibers. *Int. J. Mol. Sci.* **2019**, *20*, 960. [CrossRef]
9. Aliotta, L.; Gigante, V.; Coltelli, M.-B.; Cinelli, P.; Lazzeri, A.; Seggiani, M. Thermo-mechanical properties of PLA/short flax fiber biocomposites. *Appl. Sci.* **2019**, *9*, 3797. [CrossRef]
10. Khoo, R.Z.; Ismail, H.; Chow, W.S. Thermal and Morphological Properties of Poly (Lactic Acid)/Nanocellulose Nanocomposites. *Procedia Chem.* **2016**, *19*, 788–794. [CrossRef]
11. Oksman, K.; Aitomäki, Y.; Mathew, A.P.; Siqueira, G.; Zhou, Q.; Butylina, S.; Tanpichai, S.; Zhou, X.; Hooshmand, S. Review of the recent developments in cellulose nanocomposite processing. *Compos. Part A Appl. Sci. Manuf.* **2016**, *83*, 2–18. [CrossRef]
12. Rigotti, D.; Checchetto, R.; Tarter, S.; Caretti, D.; Rizzuto, M.; Fambri, L.; Pegoretti, A. Polylactic acid-lauryl functionalized nanocellulose nanocomposites: Microstructural, thermo-mechanical and gas transport properties. *Express Polym. Lett.* **2019**, *13*, 858–876. [CrossRef]
13. Chaerunisaa, A.Y.; Sriwidodo, S.; Abdassah, M. Microcrystalline cellulose as pharmaceutical excipient. In *Pharmaceutical Formulation Design-Recent Practices*; IntechOpen: London, UK, 2019.
14. Aliotta, L.; Gigante, V.; Cinelli, P.; Coltelli, M.-B.; Lazzeri, A. Effect of a Bio-Based Dispersing Aid (Einar® 101) on PLA-Arbocel® Biocomposites: Evaluation of the Interfacial Shear Stress on the Final Mechanical Properties. *Biomolecules* **2020**, *10*, 1549. [CrossRef] [PubMed]
15. Luzi, F.; Puglia, D.; Sarasini, F.; Tirillò, J.; Maffei, G.; Zuorro, A.; Lavecchia, R.; Kenny, J.M.; Torre, L. Valorization and extraction of cellulose nanocrystals from North African grass: Ampelodesmos mauritanicus (Diss). *Carbohydr. Polym.* **2019**, *209*, 328–337. [CrossRef] [PubMed]

16. Sessini, V.; Navarro-Baena, I.; Arrieta, M.P.; Dominici, F.; López, D.; Torre, L.; Kenny, J.M.; Dubois, P.; Raquez, J.-M.; Peponi, L. Effect of the addition of polyester-grafted-cellulose nanocrystals on the shape memory properties of biodegradable PLA/PCL nanocomposites. *Polym. Degrad. Stab.* **2018**, *152*, 126–138. [CrossRef]

17. Ghasemi, S.; Behrooz, R.; Ghasemi, I.; Yassar, R.S.; Long, F. Development of nanocellulose-reinforced PLA nanocomposite by using maleated PLA (PLA-g-MA). *J. Thermoplast. Compos. Mater.* **2018**, *31*, 1090–1101. [CrossRef]

18. Battegazzore, D.; Bocchini, S.; Alongi, J.; Frache, A.; Marino, F. Cellulose extracted from rice husk as filler for poly (lactic acid): Preparation and characterization. *Cellulose* **2014**, *21*, 1813–1821. [CrossRef]

19. Li, Z.; Reimer, C.; Wang, T.; Mohanty, A.K.; Misra, M. Thermal and Mechanical Properties of the Biocomposites of Miscanthus Biocarbon and Poly(3-Hydroxybutyrate-co-3-Hydroxyvalerate) (PHBV). *Polymers* **2020**, *12*, 1300. [CrossRef]

20. Jonoobi, M.; Harun, J.; Mathew, A.P.; Oksman, K. Mechanical properties of cellulose nanofiber (CNF) reinforced polylactic acid (PLA) prepared by twin screw extrusion. *Compos. Sci. Technol.* **2010**, *70*, 1742–1747. [CrossRef]

21. Abdulkhani, A.; Hosseinzadeh, J.; Ashori, A.; Dadashi, S.; Takzare, Z. Preparation and characterization of modified cellulose nanofibers reinforced polylactic acid nanocomposite. *Polym. Test.* **2014**, *35*, 73–79. [CrossRef]

22. Marais, A.; Kochumalayil, J.J.; Nilsson, C.; Fogelström, L.; Gamstedt, E.K. Toward an alternative compatibilizer for PLA/cellulose composites: Grafting of xyloglucan with PLA. *Carbohydr. Polym.* **2012**, *89*, 1038–1043. [CrossRef] [PubMed]

23. Oksman, K.; Mathew, A.P.; Bondeson, D.; Kvien, I. Manufacturing process of cellulose whiskers/polylactic acid nanocomposites. *Compos. Sci. Technol.* **2006**, *66*, 2776–2784. [CrossRef]

24. Melilli, G.; Carmagnola, I.; Tonda-Turo, C.; Pirri, F.; Ciardelli, G.; Sangermano, M.; Hakkarainen, M.; Chiappone, A. DLP 3D Printing Meets Lignocellulosic Biopolymers: Carboxymethyl Cellulose Inks for 3D Biocompatible Hydrogels. *Polymers* **2020**, *12*, 1655. [CrossRef] [PubMed]

25. Butchosa, N.; Zhou, Q. Water redispersible cellulose nanofibrils adsorbed with carboxymethyl cellulose. *Cellulose* **2014**, *21*, 4349–4358. [CrossRef]

26. Taheri, H.; Hietala, M.; Oksman, K. One-step twin-screw extrusion process of cellulose fibers and hydroxyethyl cellulose to produce fibrillated cellulose biocomposite. *Cellulose* **2020**, *27*, 8105–8119. [CrossRef]

27. Bondeson, D.; Mathew, A.; Oksman, K. Optimization of the isolation of nanocrystals from microcrystalline celluloseby acid hydrolysis. *Cellulose* **2006**, *13*, 171. [CrossRef]

28. Abdul Khalil, H.P.S.; Tye, Y.Y.; Leh, C.P.; Saurabh, C.K.; Ariffin, F.; Mohammad Fizree, H.; Mohamed, A.; Suriani, A.B. Cellulose reinforced biodegradable polymer composite film for packaging applications. *Bionanocompos. Packag. Appl.* **2017**, 49–69.

29. Haafiz, M.K.M.; Hassan, A.; Khalil, H.P.S.A.; Fazita, M.R.N.; Islam, M.S.; Inuwa, I.M.; Marliana, M.M.; Hussin, M.H. Exploring the effect of cellulose nanowhiskers isolated from oil palm biomass on polylactic acid properties. *Int. J. Biol. Macromol.* **2016**, *85*, 370–378. [CrossRef] [PubMed]

30. Sanchez-Garcia, M.D.; Lagaron, J.M. On the use of plant cellulose nanowhiskers to enhance the barrier properties of polylactic acid. *Cellulose* **2010**, *17*, 987–1004. [CrossRef]

31. Armentano, I.; Fortunati, E.; Burgos, N.; Dominici, F.; Luzi, F.; Fiori, S.; Jiménez, A.; Yoon, K.; Ahn, J.; Kang, S.; et al. Processing and characterization of plasticized PLA/PHB blends for biodegradable multiphase systems. *Express Polym. Lett.* **2015**, *9*, 583–596. [CrossRef]

32. Gigante, V.; Coltelli, M.-B.; Vannozzi, A.; Panariello, L.; Fusco, A.; Trombi, L.; Donnarumma, G.; Danti, S.; Lazzeri, A. Flat Die Extruded Biocompatible Poly(Lactic Acid) (PLA)/Poly(Butylene Succinate) (PBS) Based Films. *Polymers* **2019**, *11*, 1857. [CrossRef] [PubMed]

33. Darie-Niţǎ, R.N.; Vasile, C.; Irimia, A.; Lipşa, R.; Râpǎ, M. Evaluation of some eco-friendly plasticizers for PLA films processing. *J. Appl. Polym. Sci.* **2016**, *133*, 1–11. [CrossRef]

34. Maiza, M.; Benaniba, M.T.; Quintard, G.; Massardier-Nageotte, V. Biobased additive plasticizing Polylactic acid (PLA). *Polimeros* **2015**, *25*, 581–590. [CrossRef]

35. Kloser, E.; Gray, D.G. Surface grafting of cellulose nanocrystals with poly (ethylene oxide) in aqueous media. *Langmuir* **2010**, *26*, 13450–13456. [CrossRef] [PubMed]

36. Cheng, D.; Wen, Y.; Wang, L.; An, X.; Zhu, X.; Ni, Y. Adsorption of polyethylene glycol (PEG) onto cellulose nano-crystals to improve its dispersity. *Carbohydr. Polym.* **2015**, *123*, 157–163. [CrossRef]

37. Teixeira, S.; Eblagon, K.M.; Pereira, M.F.R.; Figueiredo, J.L. Towards Controlled Degradation of Poly(lactic) Acid in Technical Applications. *C* **2021**, *7*, 42.

38. Stark, N.M.; Wei, L.; Sabo, R.C.; Reiner, R.R.; Matuana, L.M. Effect of freeze-drying on the morphology of dried cellulose nanocrystals (CNCs) and tensile properties of poly (lactic) acid-CNC composites. In Proceedings of the ANTEC®2018-society of plastics engineers. 5p, Orlando, FL, USA, 7–10 May 2018.

39. Zimmermann, M.V.G.; Borsoi, C.; Lavoratti, A.; Zanini, M.; Zattera, A.J.; Santana, R.M.C. Drying techniques applied to cellulose nanofibers. *J. Reinf. Plast. Compos.* **2016**, *35*, 628–643. [CrossRef]

40. Matsuo, M.; Umemura, K.; Kawai, S. Kinetic analysis of color changes in cellulose during heat treatment. *J. Wood Sci.* **2012**, *58*, 113–119. [CrossRef]

41. Fischer, E.W.; Sterzel, H.J.; Wegner, G. Investigation of the structure of solution grown crystals of lactide copolymers by means of chemical reactions. *Kolloid-Z. Z. Polym.* **1973**, *251*, 980–990. [CrossRef]

42. Vacche, S.D.; Vitale, A.; Bongiovanni, R. Photocuring of epoxidized cardanol for biobased composites with microfibrillated cellulose. *Molecules* **2019**, *24*, 3858. [CrossRef]

43. Yao, X.; Qi, X.; He, Y.; Tan, D.; Chen, F.; Fu, Q. Simultaneous reinforcing and toughening of polyurethane via grafting on the surface of microfibrillated cellulose. *ACS Appl. Mater. Interfaces* **2014**, *6*, 2497–2507. [CrossRef] [PubMed]

44. Karim, Z.; Svedberg, A. Controlled retention and drainage of microfibrillated cellulose in continuous paper production. *New J. Chem.* **2020**, *44*, 13796–13806. [CrossRef]

45. Cinar Ciftci, G.; Larsson, P.A.; Riazanova, A.V.; Øvrebø, H.H.; Wågberg, L.; Berglund, L.A. Tailoring of rheological properties and structural polydispersity effects in microfibrillated cellulose suspensions. *Cellulose* **2020**, *27*, 9227–9241. [CrossRef]

46. Larsson, P.A.; Riazanova, A.V.; Cinar Ciftci, G.; Rojas, R.; Øvrebø, H.H.; Wågberg, L.; Berglund, L.A. Towards optimised size distribution in commercial microfibrillated cellulose: A fractionation approach. *Cellulose* **2019**, *26*, 1565–1575. [CrossRef]

47. Li, M.-C.; Wu, Q.; Song, K.; Lee, S.; Qing, Y.; Wu, Y. Cellulose nanoparticles: Structure–morphology–rheology relationships. *ACS Sustain. Chem. Eng.* **2015**, *3*, 821–832. [CrossRef]

48. Aliotta, L.; Cinelli, P.; Coltelli, M.B.; Lazzeri, A. Rigid filler toughening in PLA-Calcium Carbonate composites: Effect of particle surface treatment and matrix plasticization. *Eur. Polym. J.* **2019**, *113*, 78–88. [CrossRef]

49. Scatto, M.; Salmini, E.; Castiello, S.; Coltelli, M.B.; Conzatti, L.; Stagnaro, P.; Andreotti, L.; Bronco, S. Plasticized and nanofilled poly(lactic acid)-based cast films: Effect of plasticizer and organoclay on processability and final properties. *J. Appl. Polym. Sci.* **2013**, *127*, 4947–4956. [CrossRef]

50. Muller, J.; Jiménez, A.; González-Martínez, C.; Chiralt, A. Influence of plasticizers on thermal properties and crystallization behaviour of poly(lactic acid) films obtained by compression moulding. *Polym. Int.* **2016**, *65*, 970–978. [CrossRef]

51. Baiardo, M.; Frisoni, G.; Scandola, M.; Rimelen, M.; Lips, D.; Ruffieux, K.; Wintermantel, E. Thermal and mechanical properties of plasticized poly(L-lactic acid). *J. Appl. Polym. Sci.* **2003**, *90*, 1731–1738. [CrossRef]

52. Haafiz, M.K.M.; Hassan, A.; Zakaria, Z.; Inuwa, I.M.; Islam, M.S.; Jawaid, M. Properties of polylactic acid composites reinforced with oil palm biomass microcrystalline cellulose. *Carbohydr. Polym.* **2013**, *98*, 139–145. [CrossRef]

53. Qu, P.; Gao, Y.; Wu, G.; Zhang, L. Nanocomposites of poly (lactic acid) reinforced with cellulose nanofibrils. *BioResources* **2010**, *5*, 1811–1823.

54. Kvien, I.; Tanem, B.S.; Oksman, K. Characterization of cellulose whiskers and their nanocomposites by atomic force and electron microscopy. *Biomacromolecules* **2005**, *6*, 3160–3165. [CrossRef] [PubMed]

55. Yang, J.; Pan, H.; Li, X.; Sun, S.; Zhang, H.; Dong, L. A study on the mechanical, thermal properties and crystallization behavior of poly(lactic acid)/thermoplastic poly(propylene carbonate) polyurethane blends. *RSC Adv.* **2017**, *7*, 46183–46194. [CrossRef]

56. Eyholzer, C.; Tingaut, P.; Zimmermann, T.; Oksman, K. Dispersion and Reinforcing Potential of Carboxymethylated Nanofibrillated Cellulose Powders Modified with 1-Hexanol in Extruded Poly(Lactic Acid) (PLA) Composites. *J. Polym. Environ.* **2012**, *20*, 1052–1062. [CrossRef]

57. Chu, Y.; Sun, Y.; Wu, W.; Xiao, H. Dispersion Properties of Nanocellulose: A Review. *Carbohydr. Polym.* **2020**, *250*, 116892. [CrossRef]

58. Mariano, M.; El Kissi, N.; Dufresne, A. Cellulose nanocrystals and related nanocomposites: Review of some properties and challenges. *J. Polym. Sci. Part B Polym. Phys.* **2014**, *52*, 791–806. [CrossRef]

59. Sudharsan Reddy, K.; Prabhakar, M.N.; Kumara Babu, P.; Venkatesulu, G.; Kumarji Rao, U.S.; Chowdoji Rao, K.; Subha, M.C.S. Miscibility Studies of Hydroxypropyl Cellulose/Poly(Ethylene Glycol) in Dilute Solutions and Solid State. *Int. J. Carbohydr. Chem.* **2012**, *2012*, 1–9. [CrossRef]

60. Popa, E.E.; Rapa, M.; Popa, O.; Mustatea, G.; Popa, V.I.; Mitelut, A.C.; Popa, M.E. Polylactic acid/cellulose fibres based composites for food packaging applications. *Mater. Plast* **2017**, *54*, 673–677. [CrossRef]

61. Halász, K.; Csóka, L. Plasticized Biodegradable Poly(lactic acid) Based Composites Containing Cellulose in Micro- and Nanosize. *J. Eng.* **2013**, *2013*, 329379. [CrossRef]

62. Wang, Q.; Ji, C.; Sun, J.; Zhu, Q.; Liu, J. Structure and properties of Polylactic acid biocomposite films reinforced with cellulose Nanofibrils. *Molecules* **2020**, *25*, 3306. [CrossRef] [PubMed]

63. Aliotta, L.; Gazzano, M.; Lazzeri, A.; Righetti, M.C. Constrained amorphous interphase in poly(l-lactic acid): Estimation of the Tensile elastic modulus. *ACS Omega* **2020**, *5*, 20890–20902. [CrossRef]

64. Cicogna, F.; Coiai, S.; De Monte, C.; Spiniello, R.; Fiori, S.; Franceschi, M.; Braca, F.; Cinelli, P.; Fehri, S.M.K.; Lazzeri, A.; et al. Poly(lactic acid) plasticized with low-molecular-weight polyesters: Structural, thermal and biodegradability features. *Polym. Int.* **2017**, *66*, 761–769. [CrossRef]

65. Li, D.; Jiang, Y.; Lv, S.; Liu, X.; Gu, J.; Chen, Q.; Zhang, Y. Preparation of plasticized poly (lactic acid) and its influence on the properties of composite materials. *PLoS ONE* **2018**, *13*, e0193520. [CrossRef] [PubMed]

66. Oguz, O.; Candau, N.; Demongeot, A.; Citak, M.K.; Cetin, F.N.; Stoclet, G.; Michaud, V.; Menceloglu, Y.Z. Poly(lactide)/cellulose nanocrystal nanocomposites by high-shear mixing. *Polym. Eng. Sci.* **2021**, *61*, 1028–1040. [CrossRef]

67.   Gigante, V.; Cinelli, P.; Righetti, M.C.; Sandroni, M.; Polacco, G.; Seggiani, M.; Lazzeri, A. On the use of biobased waxes to tune thermal and mechanical properties of polyhydroxyalkanoates– bran biocomposites. *Polymers* **2020**, *12*, 2615. [CrossRef]

68.   Rahim, N.A.A.; Ariff, Z.M.; Ariffin, A.; Jikan, S.S. Study on effect of filler loading on the flow and swelling behaviors of polypropylene-kaolin composites using single-screw extruder. *J. Appl. Polym. Sci.* **2011**, *119*, 73–83. [CrossRef]